Fiber Optic Vibration Sensors for Structural Control Applications

W.B. Spillman, Jr.
B.R. Kline
Hercules Aerospace Company
Aircraft Systems Division
Vergennes, Vermont 05491

Abstract

In order to control the behavior of aerospace structures in real time, closed loop control systems require highly accurate measurements of the vibrational frequencies and amplitudes exhibited by structures at any given instant. Traditionally, this has meant the use of a large number of accelerometers mounted at various locations on the structure. The motion of the structure has then been inferred from these point measurements. Developments in the field of fiber optic sensing have now reached the point at which practical sensors may provide a near term ability to produce an output proportional to the integrated structural deformation along an attached or embedded optical fiber. In this paper, the principles of operation of two candidate techniques are discussed: polarimetric and statistical mode sensing. Experimental results are presented and compared with theoretical predictions. Finally, the advantages and limitations of integrating vs point vibration measurements are covered, with an emphasis on structural control applications.

Introduction

The one dimensional, flexible nature of optical fibers makes them almost ideal for use as distributed sensors. A parameter of the fiber that can be easily affected by a stimulus is the optical path length and a change in optical path length can be measured with great resolution using interferometric techniques. Figure 1 shows a two arm optical fiber interferometer that is sensitive to optical path length differences of less than a wavelength of light (<1 micron). Unfortunately, this is much too sensitive for stable operation without complex compensation schemes. The sensors described in this paper reduce the unwanted sensitivity by having all the arms of the interferometer in the same fiber.

A polarimetric sensor results when the two arms of the interferometer are the two orthogonal polarization modes of a single mode fiber. Any stimulus that induces a birefringence in the fiber will effectively cause a difference in optical path lengths. The polarimetric sensor considered here uses stress caused by bending to produce the birefringence. With a coherent light source at one end of the fiber and an analyzer at the other, a bend modulated signal is observed.

A statistical mode sensor (SMS) results when the interferometer has many arms, all coexisting as propagation modes within a single multimode fiber. When the output from a multimode optical fiber is projected upon a screen, a uniform circular pattern is observed. When the light is incoherent, there is a smooth distribution of intensity within the pattern. When coherent light is used, however, the pattern becomes very granular and consists of a very large number of "speckles" of varying intensities as seen in Figure 2. This is the complex interference pattern of a many armed interferometer. The distribution of these speckles changes slowly over time, but the intensity of the total circular pattern remains basically constant. When the optical fiber carrying the coherent light is perturbed, the distribution of the speckle intensities is seen to change with the perturbation, with some speckles becoming brighter, some dimmer, and some not changing at all. The total intensity of the pattern remains unchanged, however. A statistical analysis of the changes in the speckle pattern output from the optical fiber can then be used to obtain information about the perturbation of the fiber.

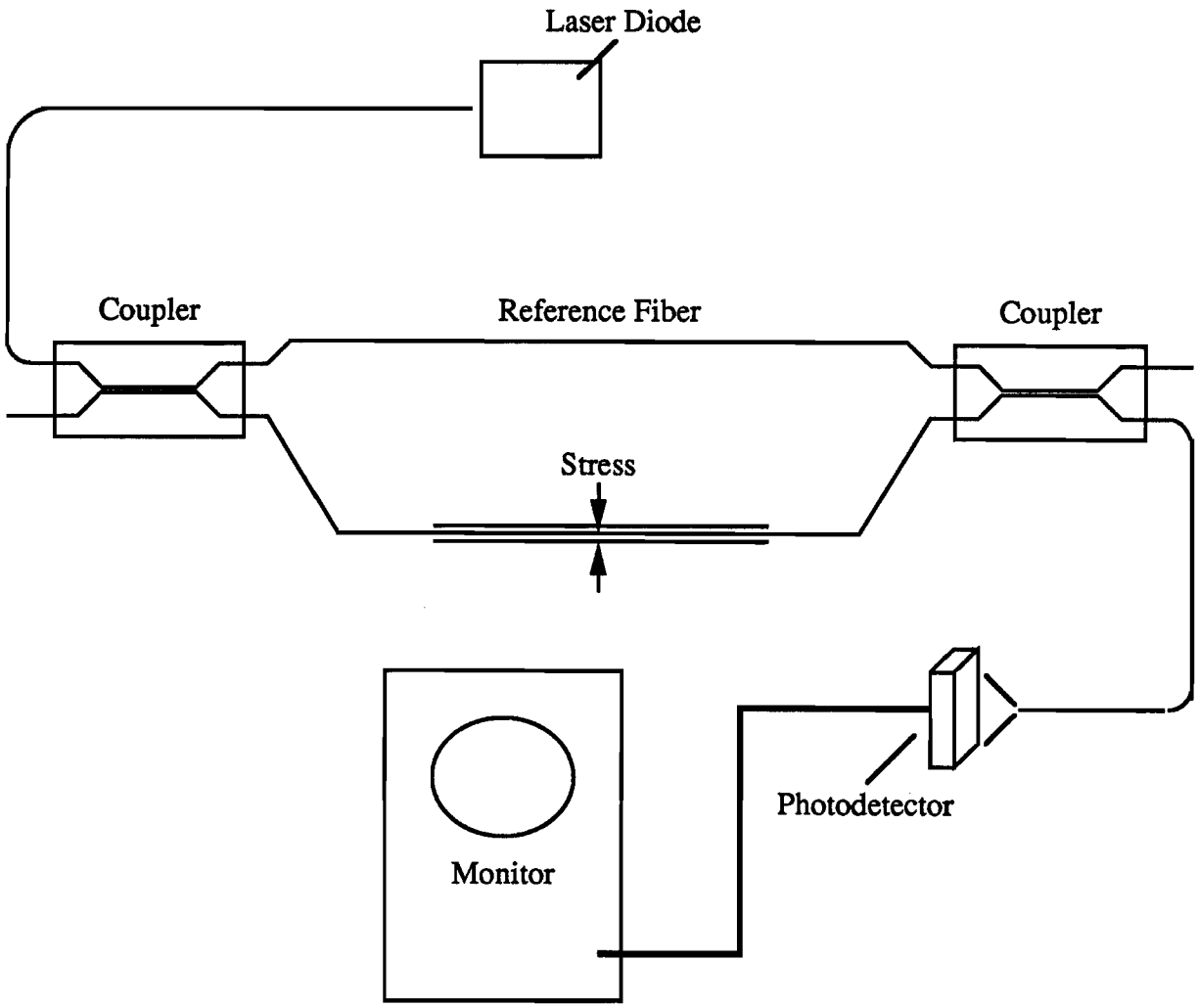

Fig. 1. Fiber optic interferometer.

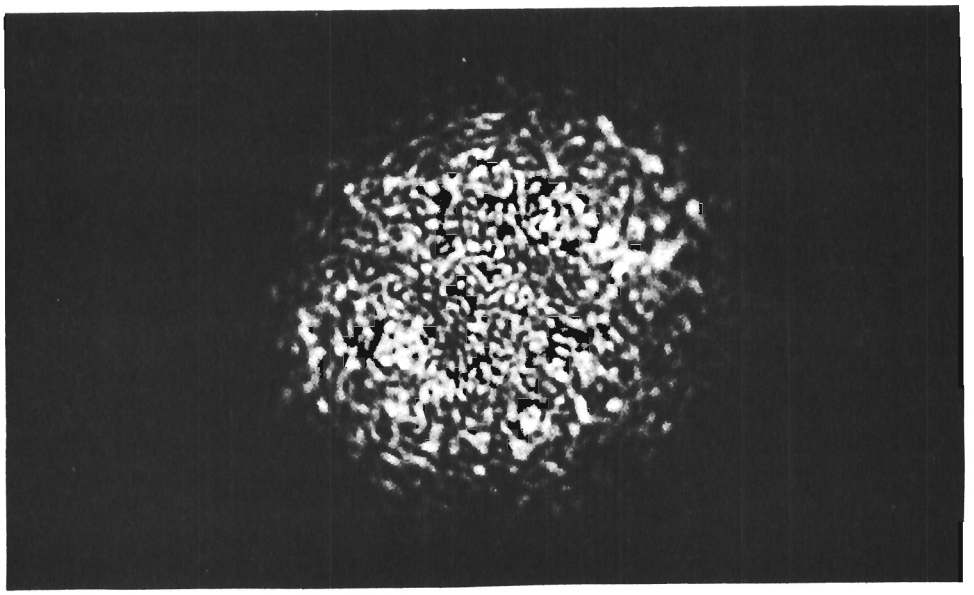

Fig. 2. Multimode optical fiber speckle emission.

There exists a body of prior work involved with investigation and use of the output speckle pattern from multimode optical fibers for a variety of purposes. Of particular interest is the work done by Claus et al. [1-2] on the vibration sensing effects using low number of modes step index optical fiber sensors. This work fills the gap between the two mode polarimetric sensor and the many mode statistical mode sensor.

In this paper, the theory and use of distributed fiber optic vibration sensors is described. In one implementation of a statistical mode sensor (SMS-A), simple spatial filtering is used to optically process the speckle pattern to provide an output related to fiber perturbation. In a second, more sophisticated implementation (SMS-B), the pattern is projected on a CCD array detector whose output is used to process changes in the pattern distribution to allow for accurate correlation with fiber perturbation. Theoretical analysis of the output modal pattern of a highly moded step index optical fiber is utilized to create a mathematical model of the SMS implementations. The mathematical model is then used to make predictions of SMS performance. Two implementations of the sensor are then simulated via a computer program. The computer simulation and actual device performance are compared with theoretical predictions. Experimental results are shown indicating the operational characteristics of the SMS units in a simple field test environment. Finally, a polarimetric sensor is described and its operation is compared to the statistical mode sensors.

Applications for distributed fiber optic vibration sensors include, but are not limited to, intrusion detection, structural vibration sensing, and acoustic sensing. A distributed sensor may be of particular importance where the alternative is a large number of point sensors such as on large space structures.

Theory: Polarimetric Sensor.

Polarimetric sensors have been well described in the literature and have been used to sense a number of different stimuli such as magnetic fields and sound waves. A concise mathematical treatment of this type of sensor is given by Beasley et al. [3] in relation to a hydrophone.

A block diagram of a polarimetric sensor is shown in Figure 3. It consists of a source of polarized light, a length of fiber with a portion exposed to a source of stress, and an output polarizer which acts as an analyzer. By choosing a coordinate system that is referenced to the applied stress, the input polarized light can be expressed (using Jones calculus) as

$$\vec{E}_{in} = \begin{bmatrix} E_x \\ E_y \end{bmatrix} = E_o \begin{bmatrix} \cos\theta \\ \sin\theta \end{bmatrix}, \qquad (1)$$

where E_o is the magnitude of the field and θ is the orientation of the polarization relative to the applied stress.

The fiber itself can be modeled by the transformation matrix

$$R = \begin{bmatrix} e^{i(\alpha/2)\cos\omega} & -e^{i(q/2)\sin\omega} \\ e^{-i(q/2)\sin\omega} & e^{-i(\alpha/2)\cos\omega} \end{bmatrix}, \qquad (2)$$

where q is the retardation of the coupled light, ω is the percentage of light coupled between the axes, and α is the phase difference between the two polarization modes given by

$$\alpha = \alpha_o + \frac{2\pi LC}{\lambda}(\sigma_x - \sigma_y) \qquad (2a)$$

where α_o is the static component, L is the length of fiber exposed to stress, C is stress-optic coefficient, λ is the wavelength of light, and σ_x and σ_y are the orthogonal radial components of the applied stress.

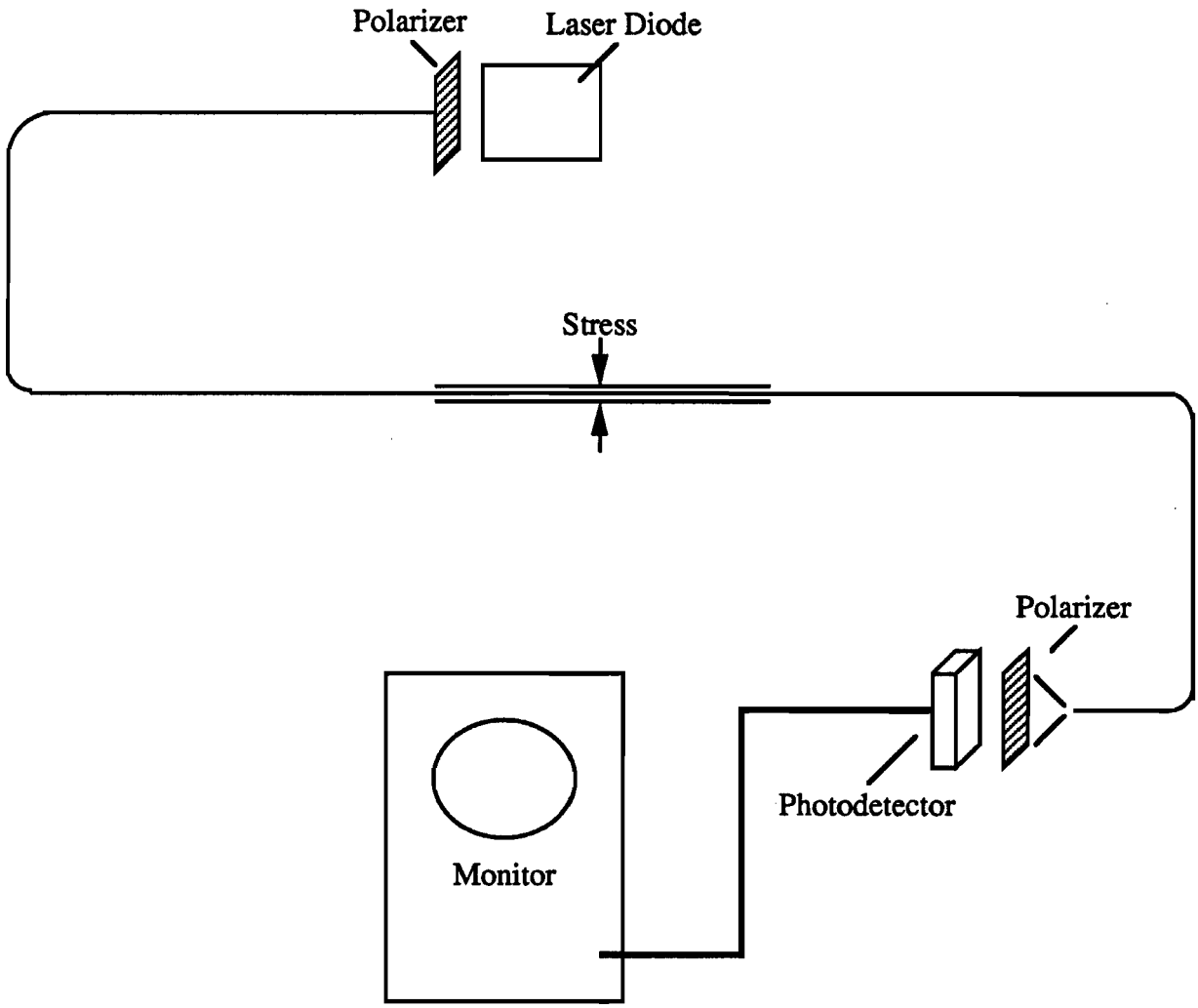

Fig. 3. Polarimetric fiber optic sensor.

Similarly, the output analyzing polarizer can be modeled by the transformation matrix

$$S = \begin{bmatrix} \cos\psi & \sin\psi \\ -\varepsilon\sin\psi & \varepsilon\cos\psi \end{bmatrix} , \tag{3}$$

where ψ is the angle of the transmission axis of the polarizer and ε^2 is its extinction ratio.

The output of the analyzing polarizer is given by

$$\vec{E}_{out} = S \cdot R \cdot \vec{E}_{in} \ . \tag{4}$$

Assuming there is no mode coupling in the fiber, making ω=0, and that the output light is linearly polarized, making ε=0, the output power can be expressed as

$$I_{out}=\vec{E}_{out} \cdot \vec{E}^{*}_{out} = \frac{E_o^2}{2}\left(1+\cos 2\theta \cos 2\psi+\sin 2\theta \sin 2\psi \cos\alpha\right) \ . \tag{5}$$

Simplifying further by setting the input polarization angle and the analyzing polarizer angle to $\pi/4$ reduces the equation to

$$I_{out} = \frac{E_o^2}{2}(1- \cos\alpha) \ . \tag{6}$$

From equation (4), it can be seen that stress on the fiber which alters the birefringence which changes the factor α, will in effect modulate the light intensity. This modulation can be made fairly linear if the stress perturbations are small and if the fiber is prestressed so that α is centered about $\pi/2$.

Theory: Statistical Mode Sensor.

Assume that the light in a multimode fiber is coherent, and linearly polarized, with the direction of propagation along the z-axis, and the electric field oriented along the x-axis. Assume each speckle has an intensity that depends upon modal interference of the coherent light in the fiber. Assume that each speckle is projected upon a photodetector element and converted to an electrical signal. The changes in this signal may then be processed to obtain information about perturbations of the optical fiber. If each individual speckle intensity is given by I_i, the total intensity is roughly constant, i.e.

$$I_T=\sum_{i=1}^{N} I_i = \text{constant} \ , \tag{7}$$

where N is the number of speckles.

Next, assume that each of the N speckle intensities act like the output from individual interferometers and vary with the fiber perturbation. Each individual speckle intensity would then vary with time according to

$$I_i=A_i\left[1+B_i\left\{\cos(\delta_i)-F(t)\ \phi_i \sin(\delta_i)\right\}\right] \ . \tag{6}$$

Although these interferometers are obviously related, subsequent analysis and modeling will assume that for small enough sampling areas and large enough number of samples, that individual speckles will be weakly or randomly related in phase, amplitude and modulation depth with respect

to perturbation, i.e. $\{A_i, B_j, \phi_i$ and $\delta_i\}$ are assumed to be collections of random numbers within some limits. The degree of validity of this assumption will be determined through comparison of model predictions with experimental results.

In order to allow comparison of theory and experiment, two different ways of processing the individual I_i's are considered: (1) summing the changes of a small enough number of the signals so that statistical averaging does not produce a constant sum as shown in Figure 4 and (2) taking the sum of the absolute value of the changes in all of the signals as shown in Figure 5.

In the first case, the sum of n<<N components is taken. In addition, only the time varying components are considered. In that case,

$$\Delta I_T = \sum_{i=1}^{n} -A_i B_i \phi_i F(t) \sin(\delta_i) \tag{7a}$$

may be reduced to,

$$\Delta I_T = \sum_{i=1}^{n} C_i F(t) \sin(\delta_i) \quad . \tag{7b}$$

Since the F(t) term is independent of the sum, it can be pulled out with the result

$$\Delta I_T = \left\{ \sum_{i=1}^{n} C_i \sin(\delta_i) \right\} F(t) \, . \tag{8}$$

This expression represents the output that could be expected from a statistical mode sensor in which the intermodal interference information is optically processed by simple spatial filtering. It should be noted that Equation (8) is also an expression of conservation of the total power contained in the speckle pattern, since as n becomes very large, the term in brackets goes to zero.

For the second case, in which the absolute values of the changes of all N pixels are summed, the basic expression for the signal output is given by

$$\Delta I_T = \sum_{i=1}^{N} \left| C_i \frac{d F(t)}{dt} \sin(\delta_i) \right| , \tag{9}$$

where the absolute values of the derivatives of Equation (7) have been summed. The final signal output for this case can be written as

$$\Delta I_T = \left\{ \sum_{i=1}^{N} \left| C_i \sin(\delta_i) \right| \right\} \left| \frac{d F(t)}{dt} \right| . \tag{10}$$

The term within the brackets sums over a large number of components so that in spite of local variations in the distribution, the sum will remain at a constant value which will be defined as C. Equation (10) can then be expressed as

$$\Delta I_T = C \left| \frac{d F(t)}{dt} \right| \quad . \tag{11}$$

From Equations (8) and (11), response to a sinusoidal perturbation, sin (ωt), would be

$$\Delta I_T = \left\{ \sum_{i=1}^{n} C_i \sin(\delta_i) \right\} \sin(\omega t) \tag{12}$$

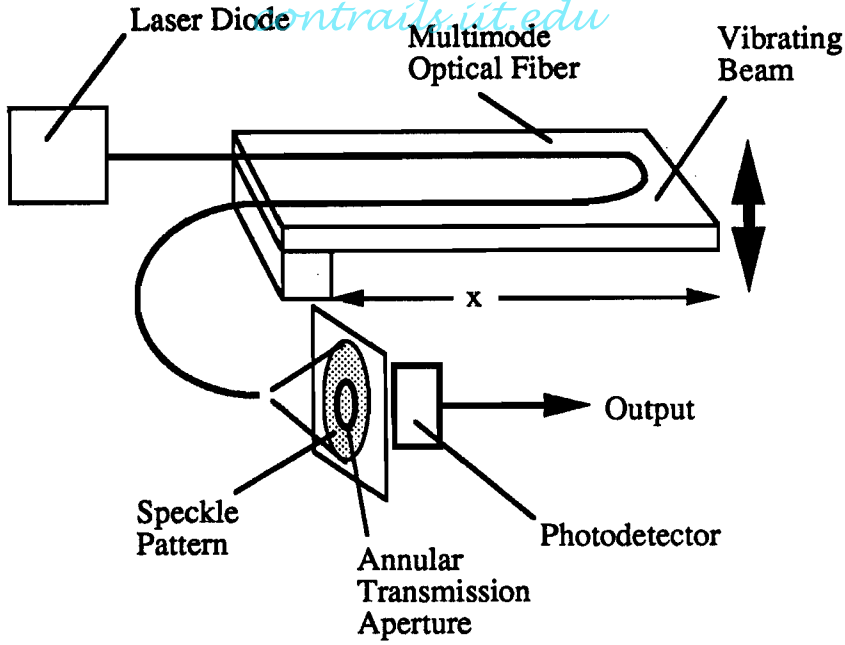

Fig. 4. SMS-A Signal Processing is accomplished using an optical spatial filter.

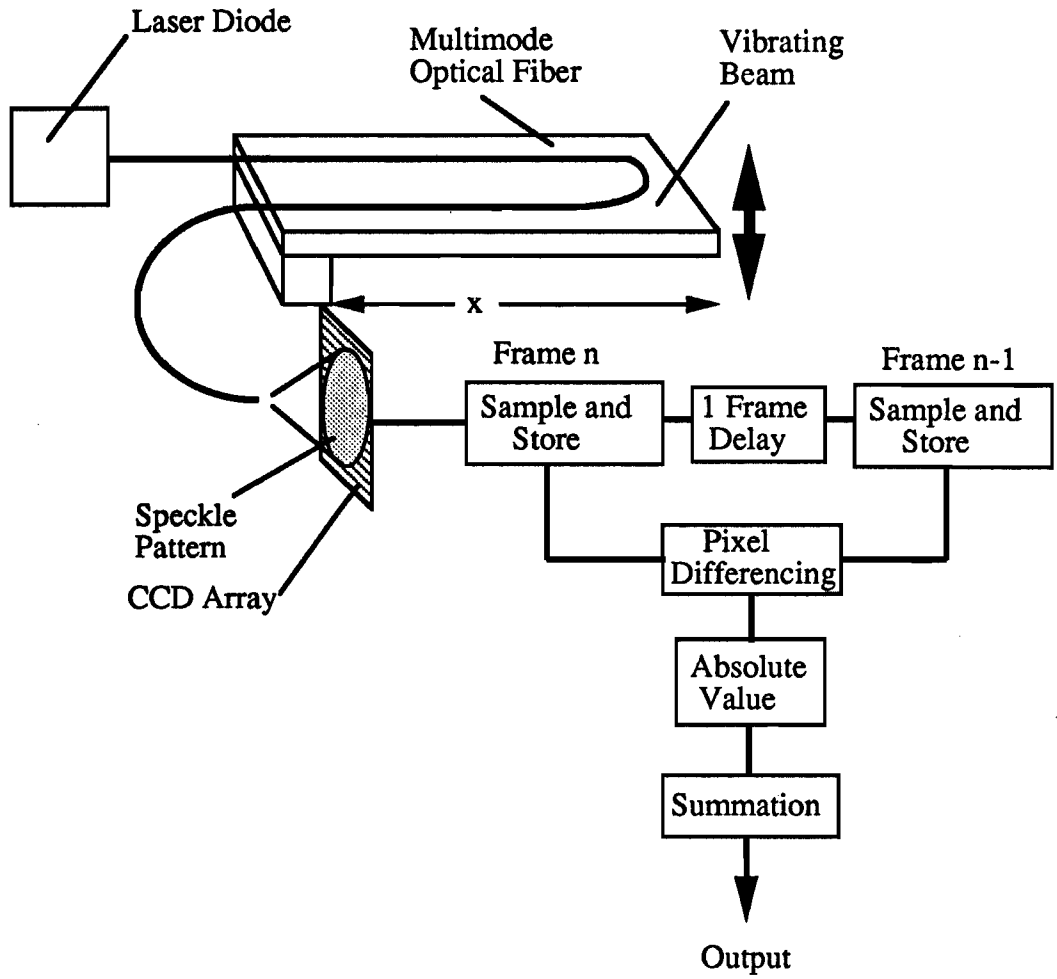

Fig. 5. SMS-B Signal processing is performed digitally by an image differentiation circuit.

for the first case, while the second case would reduce to

$$\Delta I_T = \omega\, C\,|\cos(\omega t)| \quad . \tag{13}$$

The absolute value term in Equation (13) can be replaced by an infinite sum, or

$$\Delta I_T = \omega\, C\left[\frac{2}{\pi} + \frac{4}{\pi}\sum_{k=1}^{\infty}\frac{\cos(2k\,\omega\, t)}{(4k^2-1)}\right] . \tag{14}$$

Based on Equations (11) and (14), SMS device performance when the two different processing schemes are used can be predicted. For the first case, a signal should be present at the same frequency as the perturbation and either in phase with the perturbation or π out of phase. The amplitude of the signal could range from some maximum value down to zero. For the second case, the signal has no component at the perturbation frequency, a large component at twice the perturbation frequency, and smaller components at integral multiples of twice the perturbation frequency. Although harmonic distortion exists, the signal should exhibit good amplitude and phase stability due to the statistics involved in summing the absolute value of a very large number of speckle intensity changes. In addition, due to the differentiation inherent in the second case, for constant amplitude and varying frequency perturbation, the SMS signal should exhibit a linear fall off of amplitude with decreasing frequency.

Computer Model of Statistical Mode Sensor

In order to determine the characteristics of a number (N) of interferometers with randomly related coefficients $\{A_i, B_i, \phi_i$ and $\delta_i\}$, a computer model was developed in the C language to simulate the expected output from the two different processing schemes for the statistical mode sensors. The program was written in the Lightspeed C implementation of the language and run on a Macintosh Plus computer. The language random number generator was used to provide N sets of values $\{A_i, B_i, \phi_i$ and $\delta_i\}$ to correspond to the N randomly related interferometers. The allowed ranges for the interferometer parameters were: $0.5 \geq A_i \geq 0$, $1.0 \geq B_i \geq 0$, $\pi/8 \geq \phi_i \geq 0$, and $2\pi \geq \delta_i \geq 0$. The random number generator provided the same output every time, so that any N>n set of interferometers always included the set of n interferometers generated for the smaller number.

The computer modeling produced the results shown in Figure 6. In Figure 6(a), one cycle of perturbation is applied and the normalized sums of 5, 50 and 500 pixels (interferometers) are taken. The normalization factor is the average of the sum of the pixel intensities over the one cycle. As can be seen, the fractional modulation of the pixel intensity sum decreases with increasing number of pixels, so that for 500 pixels, the modulation is negligible. Figure 6(b) depicts the result when the absolute value of each pixel change is summed over one cycle of modulation and normalized to the sum of the pixel intensities over the cycle. In this case, the signal does not change significantly as the number of pixels is increased with a modulation of ~2%.

Device Design and Fabrication

In order to test and compare the polarimetric and statistical mode sensors, three prototypes were constructed. A polarimetric sensor and two SMS signal processing designs were implemented, the SMS-A using spatial filtering to perform optical processing of the signal, and the SMS-B, which used much more sophisticated electronics in conjunction with a CCD detector.

The polarimetric sensor was assembled as shown in Figure 3 in the laboratory for comparison purposes. It consists of a laser diode light source, an input polarizer to assure a source of linearly polarized light, a length of single mode fiber of the type used for communications, an output analyzer polarizer, and a photodetector. Since the single mode fiber used was not polarization preserving, the orientations of the input and output polarizers were simply adjusted to give the best

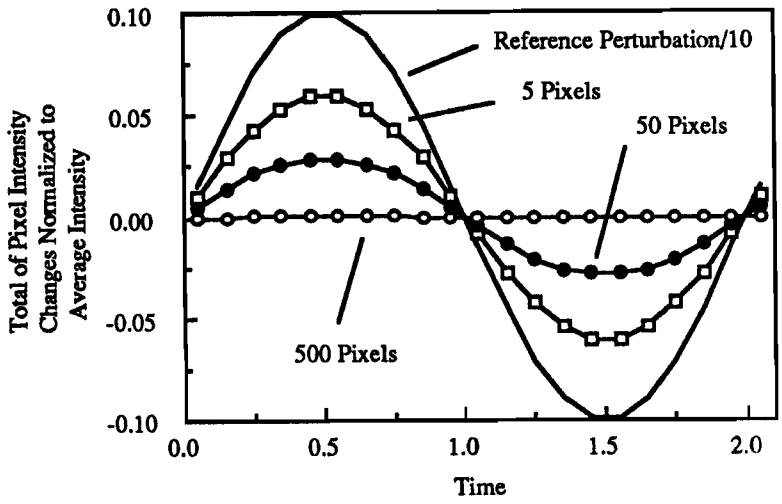

Fig. 6(a). Simulated SMS-A sensor output.

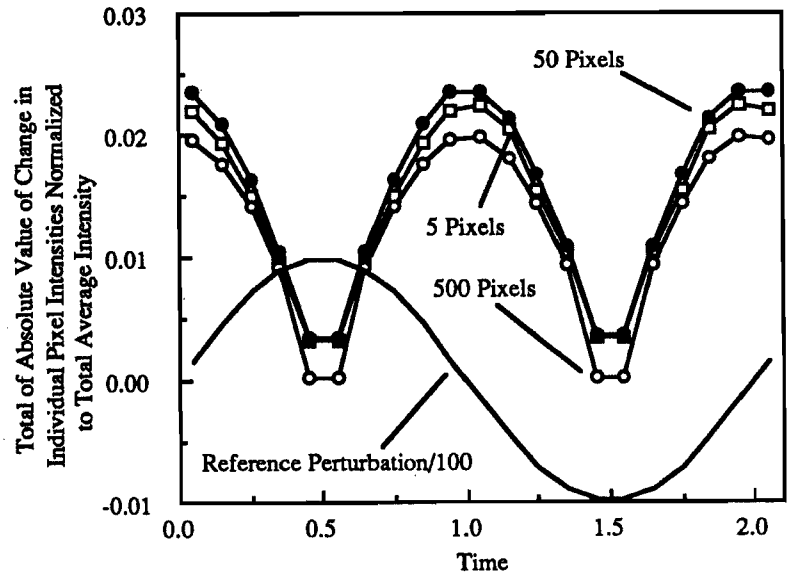

Fig. 6(b) Simulated SMS-B sensor output.

light modulation. The only signal processing required consisted of an AC coupled amplifier; a great deal of gain was needed because of the low sensitivity of the sensor.

Of greater interest were the statistical mode sensors. The SMS-A and SMS-B were designed and packaged for both lab and field use.

For the SMS-A unit, most of the speckle intensity processing is done optically, as can be seen from Figure 4. A simple amplifier for the photodetector would give a working system. Ideally, though, the output of the sensor would be much more stable and repeatable if the random effects of A_i, B_i, ϕ_i, and δ_i could be reduced. This can be done by assuming these terms vary more slowly than the perturbation signal so that they can be filtered out. Assuming a sinusoidal perturbation $F(t)= \sin(\omega t)$, and summing Equation (6) over all speckles gives a total intensity

$$I_T=\sum_{i=1}^{n}A_i+\sum_{i=1}^{n}A_i B_i\cos(\delta_i)-\sum_{i=1}^{n}A_i B_i \phi_i\sin(\omega t)\sin(\delta_i) . \qquad (15)$$

Simple high pass filtering will remove the first two terms leaving Equation (12). Because the unwanted bracketed term in Equation (12) is a gain term rather than additive, an automatic gain control (AGC) circuit is used. The control signal for the AGC circuit is derived from the inverse of the terms that were filtered out by the high pass filter. This does not provide complete compensation but A_i is completely removed and experience verifies that stability is improved. Figure 7 is a photograph of the SMS-A unit.

In the SMS-B sensor, all of the signal processing occurs in electronics as shown in Figure 5. The detector was a 128 x 128 array of photodiodes which capture an image of the speckle pattern called a frame. Each photodiode contributes one picture element, or "pixel", to the frame. Each pixel is digitized and stored in a digital memory called a frame buffer. Just before a new pixel is stored in the frame buffer, the old pixel data is removed and both old and new pixel data are passed to an arithmetic circuit. The arithmetic circuit finds the absolute value of the differences between the old and new pixels. All of the absolute values of the differences for the entire frame are then accumulated and normalized to give a single value. This single value represents the amount of change in the speckle pattern that occurs over the period of time between captured frames. For convenience, the digital value is converted back to an analog signal for display on an oscilloscope or strip chart recorder. A prototype of the SMS-B sensor is shown in Figure 8. Bandwidths in excess of 1 MHz can be attained by giving each pixel its own arithmetic circuit operating in parallel. However, to keep circuit size within reason, the photodiode array must be made much smaller. A more economical and slower method is to process the pixels serially through a single arithmetic circuit or computer. The actual implementation shown in Figure 5 clocked the pixels out of the array at 8 MHz through a pipelined "hardwired" circuit to attain a frame rate of approximately 275 Hz. The prototype unit also has an output that bypasses the final summation stage so that external signal processing may be used.

Results and Discussion

The polarimetric and the two SMS implementations were tested in a preliminary fashion in the laboratory. The tests were carried out using a communication grade single mode fiber and a 100/140 μm step index multimode optical fiber attached to a bar clamped at both ends. The fibers were attached to the bar in the same configuration as shown in Figures 4 and 5 with the single mode fiber mounted parallel to the multimode fiber. A spring weakly coupled the center of the bar to the drive piston of a Ling Dynamic Systems Linear Vibrator.

A vibrating bar was used to produce a distributed perturbation of the fiber. The choice of a bar rather than a vibrating string helped greatly with the waveform, harmonic, and phase analysis. This is because the overtones (higher modes of vibration) of a vibrating bar are not harmonic. If the overtones of the bar are excited, they would not be synchronized with the fundamental allowing them to be easily filtered out. In practice, the overtones were not present because there was no source of excitation at their frequencies. Of all the different boundary conditions for a vibrating bar

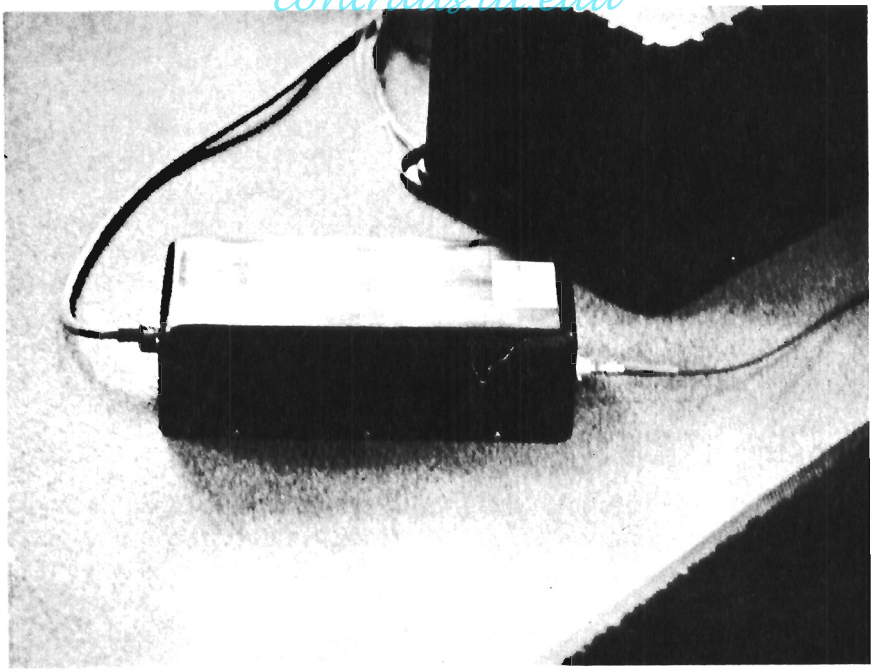

Fig. 7. SMS-A: Optical spatial filtering implementation.

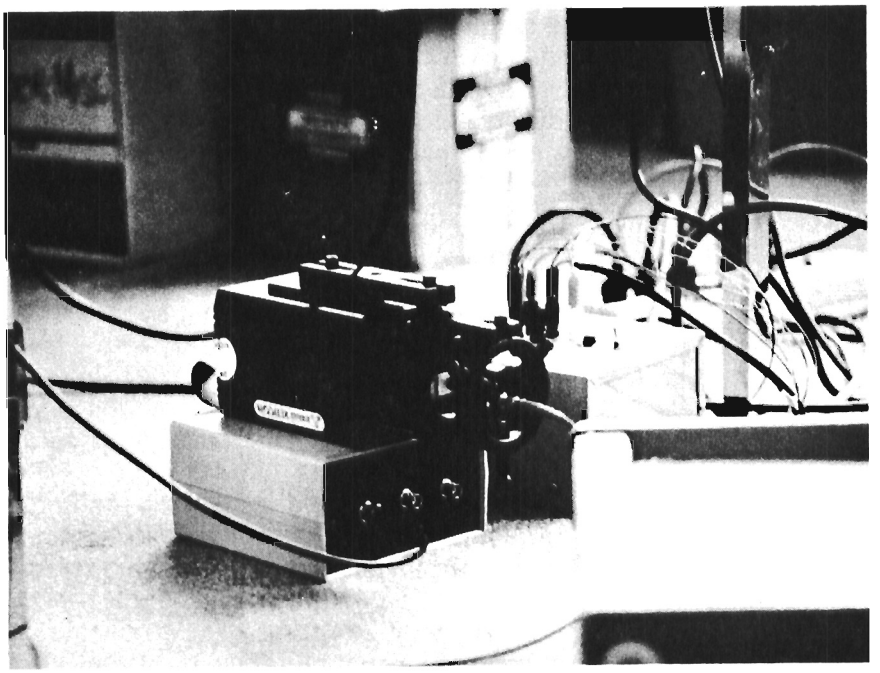

Fig. 8. Prototype SMS-B: CCD detector implementation.

(free, hinged, or clamped), the clamped - clamped configuration was chosen to avoid exciting the portion of the fiber leading up to the sensor section.

To monitor the vibrations of the bar without introducing distortions, a non-contacting fiber optic displacement sensor was used. The sensor consisted of a bundle of optical fibers whose sensing end was cleaved and polished in a uniform manner. Half of the fibers in the bundle transmitted light to the surface to be measured and the other half received the reflected light. Because the light disperses as it leaves the transmitting fiber, how much light is gathered by the receiving fibers depends on the distance to the reflecting surface.

The bar used was 74.7 cm between clamps, 0.7545 cm wide, 0.1265 cm thick, and made of steel. The fiber and glue add a little weight to the bar increasing its effective density slightly. The allowed frequencies for a bar clamped at both ends is [4]

$$\nu_n = \frac{\pi}{2l}\sqrt{\frac{Q\,\kappa^2}{\rho}}\,\beta_n^2, \qquad \kappa = \frac{a}{\sqrt{12}}, \tag{16}$$

where l is the length, Q is Young's modulus, a is the thickness, ρ is the density, and β_n are coefficients for the allowed frequencies. For the bar used

a= .321cm
l= 74.7cm
Q= 19×10^{11} dyne/cm_
d= 7.7 g/cc
and $\beta_1 = 1.5056$, $\beta_2 = 2.4997$, $\beta_3 = 3.5$, $\beta_4 = 4.5$, ...

This gives the fundamental mode at 29.4Hz which agrees with experiment. The shape of the bar as it vibrates is of the form (1-cos(x)).

The bar was first perturbed in such a way as to provide a sinusoidal output from the reference displacement sensor. This output is shown in Figure 9 along with the output from the polarimetric sensor. The three signals from the polarimetric sensor indicate the result of varying the input conditions to the fiber on the vibrating bar by wrapping the input fiber around mandrels of (a) 3.2 cm, (b) 3.8 cm, and (c) 4.4 cm. As can be seen, the polarimetric sensor is fairly immune to input conditions. As long as the bending of the input fiber does not cause enough stress to move α significantly away from $\pi/2$, Equation 6 predicts that the amplitude and phase of the output should track the excitation.

Similarly, the output from the reference displacement sensor is shown in Figure 10 along with the output from the SMS-A. The three signals from the SMS-A indicate the result of varying the input conditions to the fiber as in the previous test. By changing the input conditions, the amplitude and sign of the sum term in Equation (8) have been modified so that curve (a) is π out of phase with the bar displacement with large amplitude, curve (b) is π out of phase with the bar displacement with lower amplitude, and curve (c) is in phase with the bar displacement and has large amplitude. These results indicate that the mathematical model used to predict the behavior of SMS type sensors has reasonable validity.

Following these tests, the SMS-B sensor was tested using the same optical source, sensing fiber, and excitation configuration. These results are shown in Figure 11. In this case, the frequency of the SMS-B sensor is twice the excitation frequency, precisely in accordance with prediction but out of phase by 31^{o}. When the input conditions were varied in exactly the same manner as for the SMS-A sensor, the resulting output did not change in either amplitude or phase. These results provide additional demonstration of the validity of the simple mathematical model of device operation developed in this paper.

As Figure 11 shows, although the SMS-B maintains a constant phase, this phase is not $\pi/2$ as predicted. The large phase lag is actually a fixed time delay caused by the pipelined architecture of

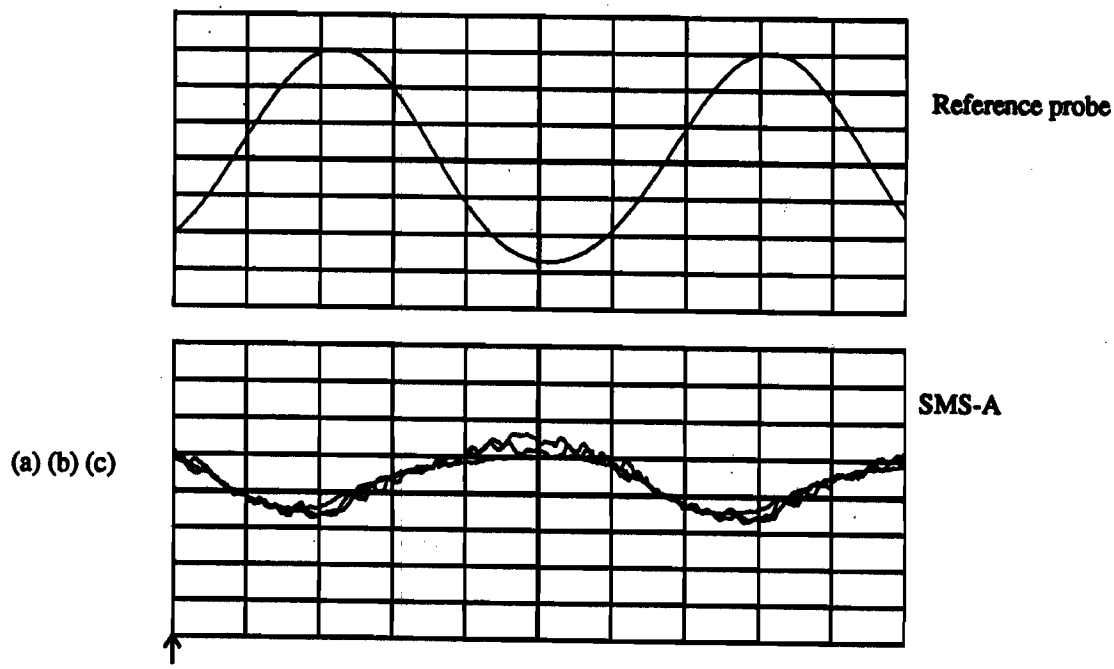

Fig. 9. Effects of varying input conditions to polarimetric sensor.

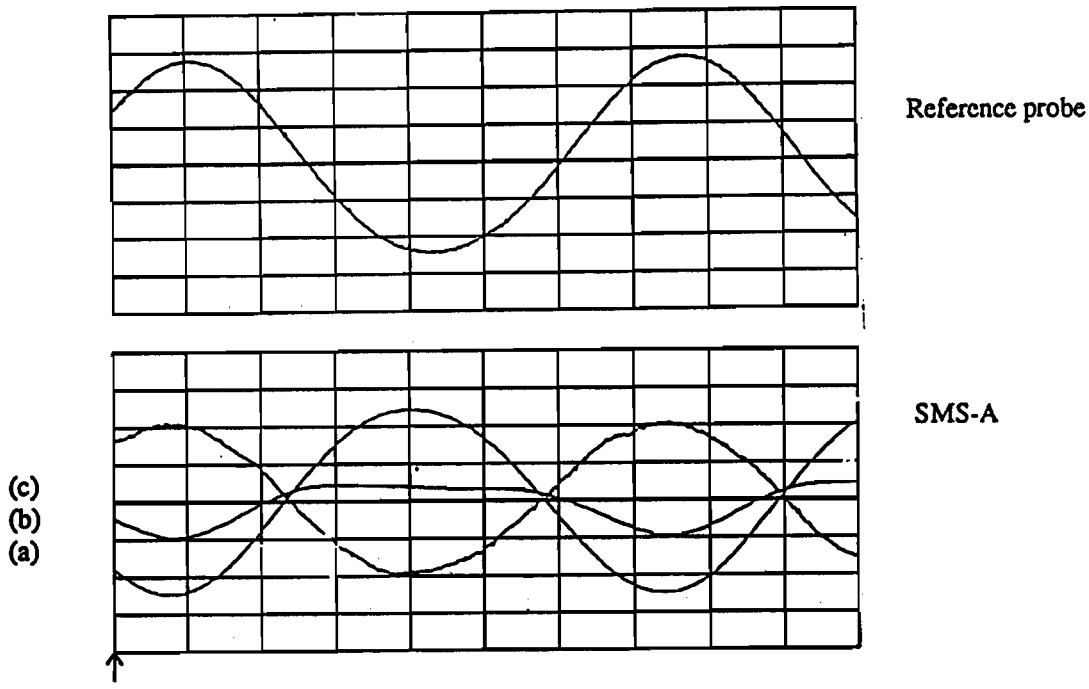

Fig. 10. Effects of varying input conditions to SMS-A.

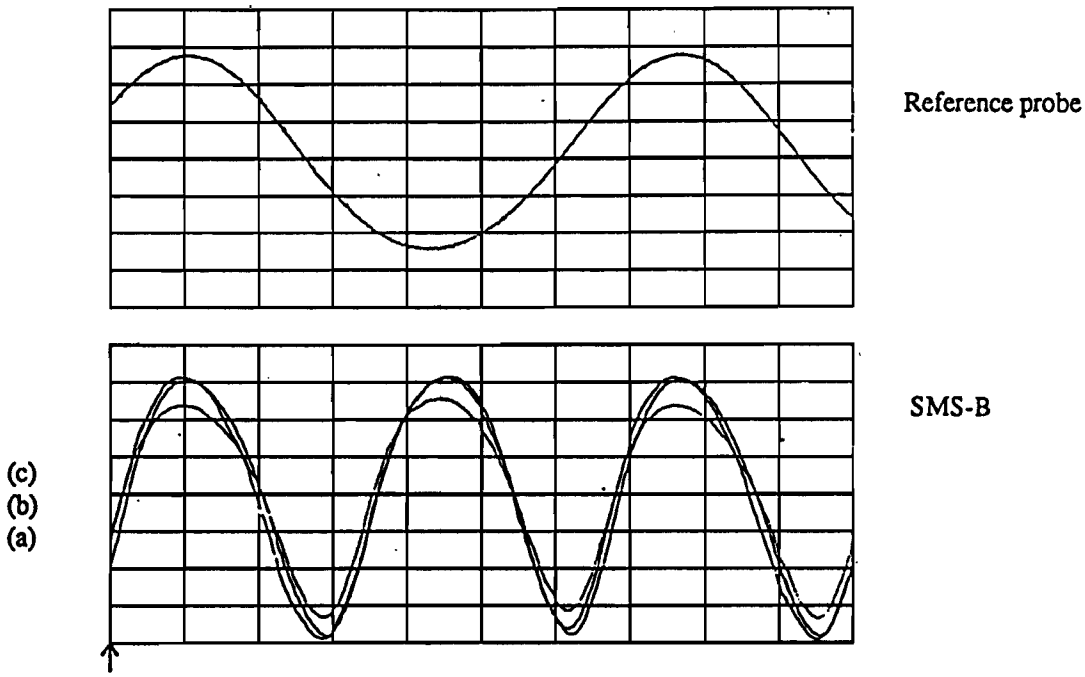

Fig. 11. Effects of varying input conditions to SMS-B.

the arithmetic circuit. The camera of the SMS-B quantizes the speckle image into frames, a complete frame taking 3.975 ms. There is a delay of approximately 3 frames from the photodiode input to the analog output. This accounts for all of the measured phase delay within the SMS-B electronics unit to within $\pm 2^{o}$. The SMS-A electronics unit has no source of large phase shift and measurement confirmed this to within $\pm 2^{o}$.

The amplitude variation of the SMS-B signal at 60.8 Hz as a function of the change in amplitude of the vibrating bar as measured by the reference sensor is shown in Figure 12. The dependence is linear as expected. Finally, Figure 13 shows the ratio of the SMS-B signal output at 2ω to the reference sensor output at ω as a function of ω. As can be seen, there is a falloff at frequencies above 65 Hz due to the frame processing rate of the SMS-B and a falloff at low frequencies due to the explicit ω dependence of the SMS-B signal as indicated by Equation (13).

A spectrum analysis of the outputs of the SMS devices was carried out under different conditions of amplitude of bar vibration. It was found that the SMS-A was very sensitive to optical input lead configuration, so that for one lead position, the fundamental frequency component virtually disappeared, leaving nothing but higher frequency harmonics. For large amplitude vibrations (4 mm), the harmonic distortion varied from 7% to 540%. Reduction of the amplitude of the vibrations by a factor of 4 (to 1 mm) resulted in a significant reduction of the harmonic distortion in roughly the same proportion although the exact numbers are not quantifiable due to the sensitivity of the SMS-A to the optical fiber lead configuration. When the SMS-B sensor was tested, it was found that the harmonic distortion ranged from 15% to 43% at the larger amplitude excitation and from 10% to 14% at the 25% excitation level.

Summary and Conclusions

Two methods of sensing vibration with integrating fiber optic sensors have been demonstrated. Mathematical models have been developed which have shown good agreement with observed sensor behavior. For the sensors examined, the sensing technique is compatible with off-the-shelf components and fiber cable and even allows for simultaneous telecommunication and sensing using the same optical fiber cable.

The results of the preliminary testing of the distributed sensors have been very encouraging. The ability to sense vibration has been demonstrated in the laboratory. Table 1 outlines the relative merits of the three sensors investigated.

Basically, the polarimetric sensor features simple construction and good amplitude, and frequency information and, with calibration, good phase response. Its main drawbacks are its low sensitivity to the type of bending stress used in our tests and the expense of coupling a laser to a single mode fiber. This sensor also exhibits a limited dynamic range because of its inherently nonlinear response as seen in Equation (6). The sensor must be adjusted to operate about a linear portion of its response curve and the excitations must be kept small to avoid amplitude errors and harmonic distortion.

The SMS-A type sensor offers the advantage that it is relatively simple and cost effective to implement. Spectrum analysis of its output can be used to determine the vibrational frequencies of whatever the sensing fiber is attached to or embedded in. This type of sensor is limited in that it can only be used to provide accurate information about vibrational frequencies, information about phase with an ambiguity of π, and no consistent information about amplitudes. Amplitude and phase of the output signal are very sensitive to the spatial configuration of the input and output optical leads to the sensing region, even if they are stationary, so frequent calibration is necessary is these parameters are needed. Like the polarimetric sensor, the SMS-A type sensor has a limited dynamic range because of its nonlinear response, however because of its statistical nature, the errors are not as bad (but neither are they adjustable).

The SMS-B type sensor improves upon the performance of the SMS-A sensor in two ways. First, like the polarimetric sensor, it is possible to obtain very accurate information about vibrational amplitudes, but with much greater sensitivity. However, the sensitivity is proportional to the signal's frequency which limits the band width and must be compensated for in subsequent

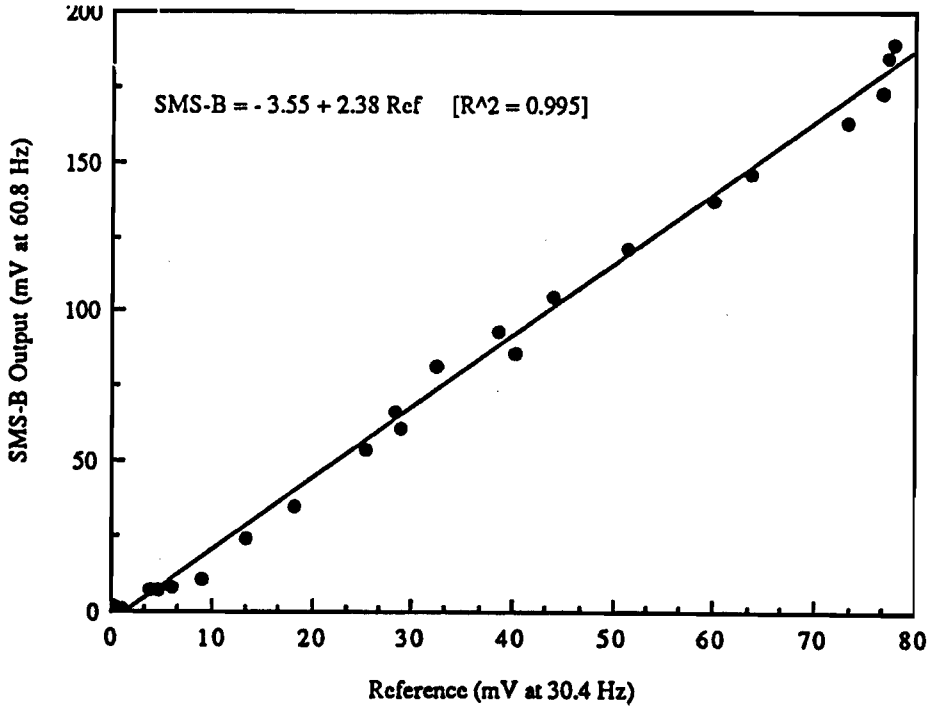

Fig. 12. SMS-B output vs. reference sensor output at constant frequency.

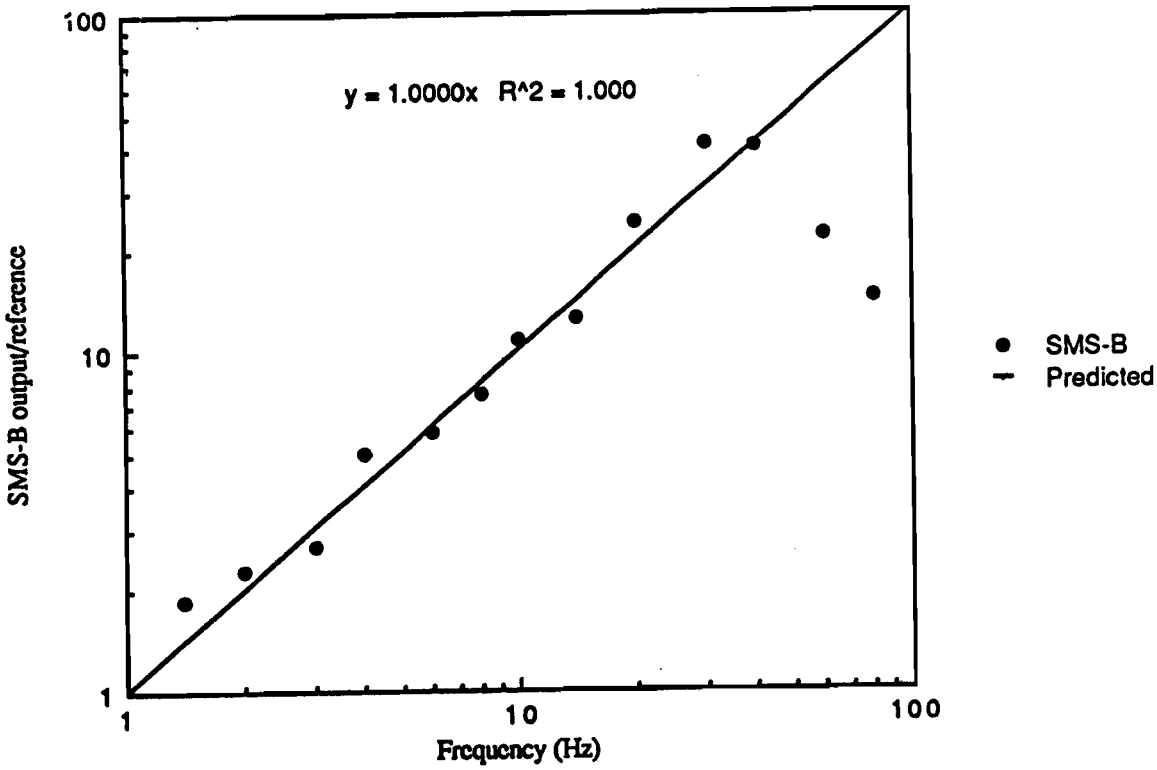

Fig. 13. SMS-B output vs. external perturbation frequency.

	Parameters						
Sensing Techniques	Sensitivity	Frequency Response	Amplitude Response	Phase Response	Harmonic Distortion	Calibration Needed	Relative Cost
Polarimetric	Low	Good (f)	Good	Good (after calibration)	Variable	Yes	Medium
SMS-A	Variable	Good (f)	Variable	Good (to within π)	Variable	Yes	Lowest
SMS-B	High	Good (2f)	Good (scales with f)	Good (to within π)	Low	No	Highest

Table 1: Comparison of Integrating Fiber Optic Vibration Sensors.

processing. Second, also like the polarimetric sensor, this type of sensor is not sensitive to the spatial configuration of the input and output optical leads to the sensing region as long as they are relatively stationary. Unlike the polarimetric and SMS-A type sensors, the dynamic range of the SMS-B type sensor is relatively large because its response is linear as Equation (11) shows. The principal limitation of the SMS-B sensor lies in the fact that it also provides phase information with an ambiguity of π because its output is frequency doubled. The phase ambiguity inherent in the SMS sensors precludes them from being straightforwardly used to provide error signals in closed loop structural control systems. Their use in such systems is still possible using sophisticated control algorithms based upon some a priori knowledge of the structural dynamics.

Both implementations of the SMS technique should have application for present sensing needs. Integrating sensors for the determination of vibrational structural modes could be used for active structural control in one application while another might include detection of structural damage or fatigue through detection of changes in basic structural vibration patterns. In applications where redundancy is needed for many point sensors, a distributed fiber optic sensor may be very cost effective if used to verify the operation of the primary sensors.

References

1. N. K. Shankaranarayanan, K. T. Srinivas, and R. O. Claus, "Mode-Mode Interference Effects in Axially strained Few-Mode Optical Fibers", SPIE Fiber Optic and Laser Sensors V (1987) **Vol. 838.**

2. K. D. Bennet, R. O. Claus, and M. J. Pinders, "Internal Monitoring of acoustic emission in graphite-epoxy composites using embedded optical fiber sensors", Proc. Quant. NDE Cof., (San Diego, Ca.), Aug 1986.

3. J. D. Beasley, D. W. Stowe, V. J. Tekippe, P. M. Kopera, and D. R. Moore, "A Sensitive Polarization Hydrophone", Proc. SPIE Fiber Optic and Laser Sensors, (Arlington, Va), April 1983.

4. P. M. Morse, Vibration and Sound, Ch. IV.15, Acoustical Society of America.